Magnetogasdynamic Effects on Acoustic Waves in MHD Generators

A. Currie Munce Jr.,* Morton Mitchner,† and J. Kent Koester‡
Stanford University, Stanford, California

The solutions of an MHD dispersion relationship have been examined to analyze the magnetogasdynamic effects on the acoustic and entropy waves in an MHD generator, with emphasis on both the magnetoacoustic phase velocities and wave amplitudes. The analysis was facilitated by the introduction of a new nondimensional frequency which incorporates the effects of frequency and the magnetic interaction parameter in one variable. To measure the relatively small effects predicted for laboratory-scale MHD generators, special experimental methods were developed based on the use of a low-frequency acoustic excitation and the analysis of the phase difference between pressure signals measured at different locations in the MHD generator. Preliminary results from experiments performed using the Stanford M-2 MHD generator facility demonstrate good agreement between the experimental data and solutions of the MHD dispersion relationship.

Introduction

FLUCTUATIONS and nonuniformities are inherent in combustion-driven MHD generators. These fluctuations and nonuniformities may result, for example, from combustor-generated noise, nonuniform mixing in the combustion process, and turbulent fluctuations in the flowfield. These inherent fluctuations can be measured as fluctuations in the plasma pressure, temperature, density, and velocity. The fluctuating quantities may be viewed as consisting of two parts: wave-like disturbances and background noise. The wave-like disturbances are of two types: 1) upstream- and downstream-traveling magnetoacoustic waves, and 2) a magnetoentropic wave that travels with a speed approximately equal to that of the gas. The wave-like part demonstrates a strong propagational character, while the noise portion tends to be dissipative with only a weak propagational character. The magnetoacoustic fluctuations are of particular interest because they involve a transport of energy which can experience a significant magnetoacoustic interaction while propagating back and forth through an MHD generator.

Fluctuations are important in MHD generators because of the strong dependence of the electrical conductivity and Hall parameter on the flow conditions. Relatively small fluctuations in the plasma temperature and pressure, for instance, can induce large nonuniformities in the plasma electrical conductivity. This dependence of the plasma properties on the wave-type disturbances provides a mechanism through which energy in the wave modes can be coupled, by means of the external circuitry, to the energy in the high-enthalpy gas. Fluctuations in fluid properties serve as sources of acoustic-like disturbances which in turn, via the electric circuits, generate further fluctuations. The existence of such a mechanism for the exchange of acoustic and electrical energy and hence the possibility of large propagating fluctuations, was first described in some early work[1-3] on magnetoacoustic interactions. Later work[4-7] suggested that for certain operating conditions this mechanism could lead to instabilities in MHD generators.

Whether instabilities develop or not, the coupling between the inherent fluctuations in an MHD generator and the electrical power circuitry is undesirable and can affect an MHD generator's performance in many different ways. Even moderate acoustic oscillations could produce large plasma nonuniformities, which would lead to degradation of an MHD generator's electrical performance. Interactions and oscillations may develop between the magnetoacoustic field and the electrical load circuitry which would affect the development of advanced power conditioning circuits. This type of interaction may already have been observed at the Component Development and Integration Facility (CDIF) in Montana during tests of the inverter circuits.[11] The understanding of the nature of the magnetoacoustic interaction is important for the future design and success of large-scale MHD power plants.

The most common method of studying the nature of the magnetoacoustic interaction analytically (and thereby obtaining predictions of wave growth or attenuation, phase velocity, etc.) has been to examine the solutions of an MHD dispersion relationship. Experimental data are needed in order to assess the validity of the analytical model and the approximations used in deriving this MHD dispersion relationship. To date, no experimental results have been reported which enable a comparison to be made with solutions of the MHD dispersion relationship. The reason for this state of affairs is that in small interaction, laboratory-scale MHD generators the predicted magnetoacoustic effects are small and often overwhelmed by competing effects.[12] To attempt to measure predicted magnetoacoustic effects, well-designed experiments with sensitive measurement techniques are needed. This paper will present the results of a series of experiments performed using the Stanford M-2 facility that clearly demonstrate the magnetoacoustic effects on the two acoustic-like waves in an MHD generator. These data can be used to assess certain aspects of the magnetacoustic theory.

Theoretical Development

Dispersion Relationship

The theoretical approach involves the solution of essentially the same MHD dispersion relationship as described by Barton et al.[7-10] It comes from a first-order linearization of the three quasi-one-dimensional MHD conservation equations for time dependent perturbations about a known steady-state solution. The linearization is done in terms of the acoustic variables p', u', T' (pressure, velocity, and temperature, respectively), and includes variations in plasma properties, such as electrical con-

Received Nov. 26, 1984; revision received May 22, 1986.

*Research Assistant, Department of Mechanical Engineering; presently, Research Staff Member, IBM Almaden Research Center. Member AIAA.

†Professor, Department of Mechanical Engineering. Member AIAA.

‡Advanced Technology Consultant, Palo Alto, CA. Member AIAA.

ductivity and chemical composition. The MHD channel is modeled as a forced boundary value problem in which all disturbances are assumed to originate either at the upstream or downstream boundaries. The linearity of this system of equations requires that fluctuations in the MHD channel always be of the same frequency as the boundary excitation source. For this reason, traveling wave solutions of the form $\exp\{i(kx-\omega t)\}$ may be assumed to satisfy the equations. The result is a cubic dispersion relationship whose roots yield three complex wavenumbers, $k=k_r+ik_i$, which are functions of the angular frequency ω and of the MHD interaction parameter S. These three complex wavenumbers represent three different types of waves: downstream magnetoacoustic, upstream magnetoacoustic, and convected magnetoentropic waves. The imaginary part of the complex wavenumber describes the magnetoacoustic effect on the amplitude of the three waves because the amplitude is proportional to $\exp(-k_i x)$. The real part of the complex wavenumber describes the magnetoacoustic effect on the phase velocity of the three waves. The phase velocity is related to the real part of the wavenumber k_r because $c_{\text{phase}}=(\omega/k)_r$.

The results from the numerical solution of this MHD dispersion relationship for conditions typical of those that can be obtained in the Stanford M-2 MHD generator facility are shown in Fig. 1 for the downstream-traveling magnetoacoustic wave (results for the other two waves are similar). In these figures, both the effect on the phase velocity and the wave amplitude are demonstrated. In these graphs, the abscissa is a nondimensional frequency particularly useful for the study of magnetoacoustics. It is expressed in terms of the angular frequency ω, length of the duct L, isentropic speed of sound a_0, magnetic interaction parameter S, and Mach number of flow M. The magnetic interaction parameter is a nondimensional number that defines the relative strength of the applied Lorentz $\boldsymbol{J}\times\boldsymbol{B}$ force to the inertial force of the fluid. For conditions typical of those in the Stanford M-2 facility, the magnitude of this nondimensional frequency is equal to one when the physical frequency is about 125 Hz.

The first graph represents the MHD effect on the phase velocity of the wave in an MHD generator. For the case of no MHD interaction, the phase velocities for the two magnetoacoustic waves and the magnetoentropic wave reduce to the well-known expressions $c_{\text{phase}}=u\pm a_0$ and $c_{\text{phase}}=u$, respectively. Here u is the fluid velocity, a_0 is the isentropic speed of sound, and the upper and lower signs apply, respectively, to downstream- and upstream-traveling acoustic waves. For the general case, it is convenient to define a wave velocity a as the difference between the phase velocity of the wave and the fluid velocity. The MHD effect on the phase velocity of a wave can then be represented by the deviation of a/a_0 from one for the two magnetoacoustic waves and the deviations from zero for the magnetoentropic wave. The dependence of the a/a_0 curves on Mach number has been found numerically to be small over a wide range of Mach numbers from 0.15 to 0.80.

In the wave amplitude graphs, the imaginary part of the wavenumber is divided by the product $(S\cdot M)$ to allow all the dependence on the magnetic interaction parameter to be explicitly displayed in these graphs. The fact that the curves are almost constant for sufficiently large values of the nondimensional frequency ω demonstrates that k_i scales linearly with S over a wide range of frequencies and interaction parameters. The effect of changes in Mach number on the values of the wave amplitudes for large $\hat{\omega}$ scales almost directly with residence time in the channel for each of these waves. For instance, for a downstream-traveling wave [phase velocity proportional to $(1+M)$] the residence time in the channel decreases as the Mach number is increased, and the large $\hat{\omega}$ value of the curve decreases proportional to changes in $(1+M)$. The parameter, which has the largest effect on both the phase velocity and wave amplitude curves, is the Faraday load factor K_F. The Faraday load factor is a nondimensional number which ranges from zero to one and is defined to be the ratio of the transverse electric field between the electrodes pairs under operating conditions to the value of the electric field under open-circuit conditions (its maximum value).

Solutions of this MHD dispersion relationship (or of similar relations) have been studied extensively,[1-7] with particular attention paid to the solution for the imaginary part of the wavenumber because the value of k_i governs the possible occurrence of MHD instabilities. An important feature that has been brought out by the present study is the introduction of the nondimensional frequency given in Fig. 1. With the use of this nondimensional frequency, the entire dependence of the solution on frequency and magnetic interaction parameter is displayed explicitly. There is no other implicit dependence on frequency or MHD interaction. This simplication will apply as long as viscous and thermal conduction effects are ignored. The physical reason for this nondimensional grouping is that for acoustic fluctuations the inertial force scales with angular frequency ω. This nondimensional grouping is then a ratio of the acoustic inertial force to the MHD $\boldsymbol{J}\times\boldsymbol{B}$ force. The use of this nondimensional frequency helps to clarify the nature of the MHD interaction, particularly at low frequencies.

Channel Acoustics

The simplest acoustic model for an MHD channel is a constant-area duct with an excitation source upstream and a known boundary condition downstream, as shown schematically in Fig. 2. The pressure field inside the duct can be described analytically by the simple acoustic wave equation, which requires two boundary conditions, one upstream and one downstream. A useful form in which to specify the downstream boundary condition is in terms of a complex

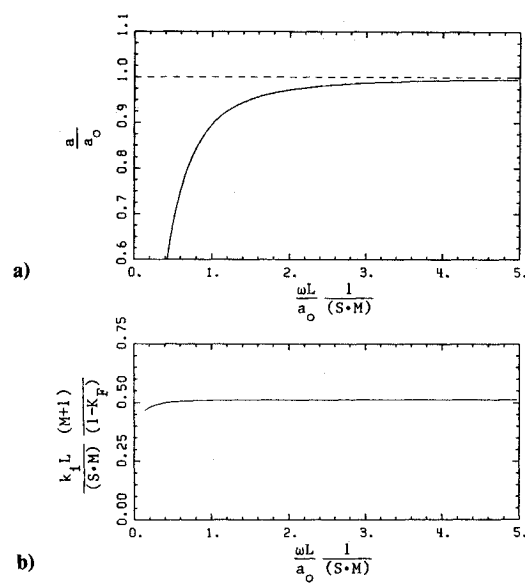

Fig. 1 Results of MHD dispersion relationship for effects on a) phase velocity and b) damping coefficient of the downstream-traveling magnetoacoustic wave.

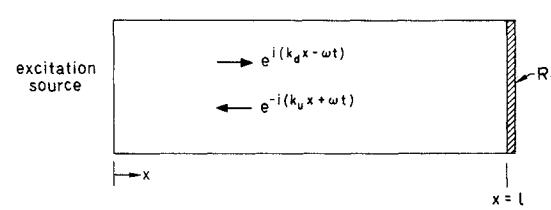

Fig. 2 Schematic of the simplest acoustic model for an MHD generator.

reflection coefficient, R_1. The upstream boundary condition must specify the nature of the upstream excitation source and how it varies in amplitude as a function of frequency.

Under ordinary acoustic conditions the solution to the wave equation yields a pressure field inside the duct that can be expressed as the superposition of a downstream- and an upstream-traveling wave

$$p'(x,t) = Ae^{i(k_d x-\omega t)} + Be^{-i(k_u x+\omega t)} \tag{1}$$

The downstream boundary condition R_1 can be used to relate the coefficients A and B in this expression by

$$R_1 = re^{i\theta} = \frac{P_{\text{up}}}{P_{\text{down}}}\bigg|_{x=\ell} = \frac{B}{A}\, e^{-i(k_u+k_d)\cdot\ell} \tag{2}$$

Equation (1) can then be rearranged in the form

$$p'(x,t) = Ae^{ik_{rd}\cdot\ell}e^{-k_{id}\cdot x}\sqrt{1+r'^2+2r'\cos[2\bar{k}(x-\ell)-\theta]}\,e^{i\phi}e^{i\omega t} \tag{3}$$

where $r' = r\,\exp\{(k_{iu}+k_{id})\cdot(x-\ell)\}$, $\bar{k} = (k_{ru}+k_{rd})/2$, and the phase angle ϕ is given by

$$\tan\phi = -\frac{r'\sin[k_{ru}(x-\ell)-\theta] - \sin[k_{rd}(x-\ell)]}{r'\cos[k_{ru}(x-\ell)-\theta] + \cos[k_{rd}(x-\ell)]} \tag{4}$$

The subscripts r and i refer to the real and imaginary parts, and the subscripts d and u refer to the downstream- and upstream-traveling acoustic-like waves, respectively.

The coefficient A in Eq. (3) can be determined once the upstream boundary condition is specified. To determine the phase of the pressure wave in the duct from Eq. (4), A is not needed and hence the upstream boundary condition is not needed. The phase anywhere in the duct is only a function of the downstream reflection boundary condition and is independent of the upstream excitation source. This property is particularly advantageous in an MHD generator where the exact nature and amplitude of the upstream source is unknown.

The phase angle as defined in Eq. (4) contains an arbitrary constant. A well-defined quantity is the phase difference between two pressure signals measured at different axial locations in the duct. For the idealized case where there are no dissipative losses ($k_i = 0$), $R_1 = 1$, and $M = 0$, this quantity depends on frequency as shown in Fig. 3. The phase difference is always 0 or 180 deg with sharp transitions in between. The reason for this behavior can be explained in terms of the envelope of the standing-wave pattern that exists in the duct. For this simple case, the envelope of the pressure fluctuations at a given frequency would look similar to that shown in Fig. 4. The downstream boundary is always an antinode if the reflection coefficient is real and positive. The locations of the nodes in this pattern correspond to the minima in the square root term in Eq. (3). In this case $\cos[2\bar{k}(x-\ell)-\theta] = -1$ or $2\bar{k}(x-\ell)-\theta = -(2n+1)\pi$ with $n = 0, \pm 1, \pm 2$, so

$$(x-\ell)_{\text{node}} = -[(2n+1)\pi-\theta]/2\bar{k} \tag{5}$$

The first node occurs for $n = 0$, and successive nodes in the standing-wave pattern correspond to incremental values of n.

The behavior of the phase difference in Fig. 3 can be understood by examining the locations of the nodes in Fig. 4 relative to the two axial measurement locations. If the two axial locations are separated by an even number of nodes, the phase difference is 0 deg; if they are separated by an odd number of nodes, the phase difference is 180 deg. The transition between 0 and 180 deg occurs when one of the measurement locations happens to be a node. The location and spacing of the nodes changes when the frequency changes as described by Eq. (5). Starting at low frequencies, the nodes are widely spaced and the two axial locations are not separated by any nodes, hence, no phase difference. As the frequency increases, all the nodes move toward the downstream boundary. The frequency at which the location of the first node is equal to that of the most upstream of the two axial locations is the frequency at which the first transition to 180 deg occurs in Fig. 3. Successive transitions occur as nodes, which continue to move closer to the downstream boundary as the frequency increases, pass by one or the other of the measurement locations. For these idealized conditions, measurements of the transition frequencies would enable the sound speed to be determined.

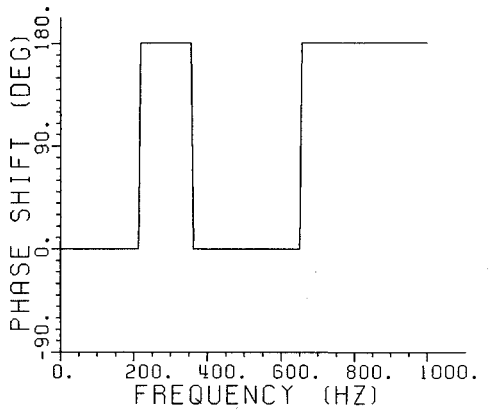

Fig. 3 Phase difference between pressure signals at two different channel locations vs frequency (for the ideal conditions $M = 0$, $R_1 = 1$, and $k_i = 0$).

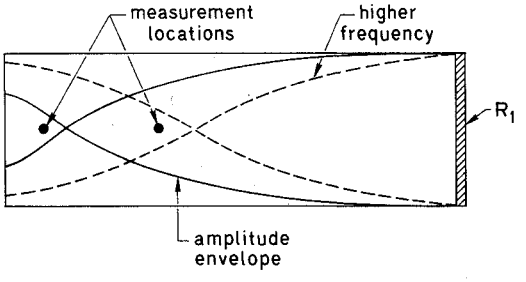

Fig. 4 Envelope of the standing-wave pressure fluctuations for two different frequencies (closed-end boundary condition).

This simple example illustrates the basic principles that underlie the experiments to be described later. Under real conditions, dissipation, mean fluid flow, and an imperfectly reflecting downstream boundary produce distortions in the idealized dependence of the phase difference on frequency; but the same basic behavior is preserved. Because of nonideal effects, the transitions are more gradual and the peak values are less than 180 deg.

Magnetoacoustic Effects on the Phase Difference

For MHD conditions, the character of the dependence of the phase difference on frequency will be influenced by the two effects shown in Fig. 1; namely the MHD effects on the phase velocity and on the damping of the acoustic-like waves. The frequency at which a sharp transition in the phase difference occurs (under idealized conditions) is directly related to the average phase velocity of the two magnetoacoustic waves. The relationship can be seen by rewriting Eq. (5) in terms of the transition frequencies that would be observed at a fixed measurement location: $\bar{k}_{\text{trans}} = [-(2n+1)\pi+\theta]/[2(x-\ell)]$, and then

$$\omega_{\text{trans}} = \bar{c}\cdot\bar{k}_{\text{trans}} = \bar{c}\,\frac{(2n+1)\pi-\theta}{2(\ell-x)}$$

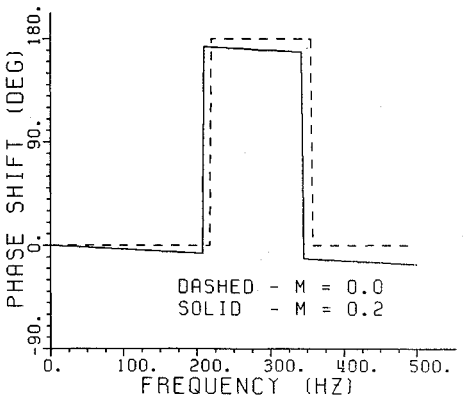

Fig. 5 Effect on the phase difference due to a mean flow velocity ($M=0.2$).

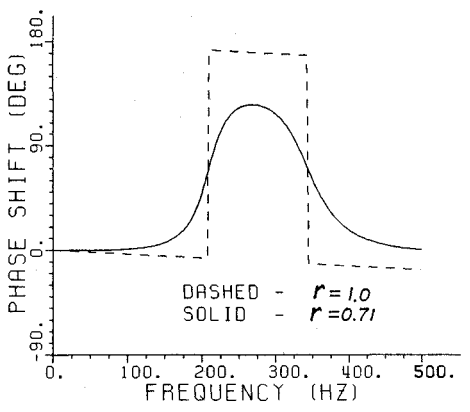

Fig. 6 Effect on the phase difference due to an imperfectly reflecting downstream boundary condition ($\theta=0$ for both curves).

One can see that that any change in $\bar{c}$ will lead directly to a shift in the transition frequency. The shift in frequency would be relatively easy to measure if the transitions in the phase difference plots were sharp. The more gradual the transitions become due to acoustic losses, the less sensitive the technique becomes for measuring changes in the average phase velocity.

Ordinary acoustic effects can cause $\bar{c}$ to change due to variations in the Mach number. The average phase velocity of the two acoustic waves is proportional to $(1-M^2)$. Any increase in the Mach number causes a reduction in $\bar{c}$ and hence causes the transition frequencies to shift to lower values. The effect that a nonzero Mach number can have on the phase difference is demonstrated in Fig. 5. The small negative slope in the $M=0.2$ curve is due to the difference in the phase velocities of the downstream- and upstream-traveling waves when there is a mean gas velocity. The shift to lower frequencies in the $M=0.2$ curve is due to a 4% reduction in the average phase velocity. Any reduction in $\bar{c}$ due to magnetoacoustic effects would cause a similar shift to lower frequencies. For the magnetoacoustic case, the reduction in $\bar{c}$ would vary strongly with frequency; the shift at the second transition would be less than at the first.

The peak values of the phase difference and the shape of the dependence on frequency in the region of the transitions are sensitive to the amount of acoustic loss in the channel. There are two sources of acoustic loss: transmission loss at the exit due to an imperfectly reflecting boundary, and dissipative losses in the flow due to viscous and thermal effects. Transmission loss affects the phase difference because it makes the value of r in Eq. (4) less than one. Figure 6 demonstrates what happens to the phase difference when the value of r is reduced from 1.0 to 0.71 [the experimental value computed from Eq. (7)]. The dissipative loss affects the phase difference because the exponential term in the expression for r' becomes less than one if k_i is greater than zero. Figure 7 demonstrates the effect of two different values of k_i on the phase difference. The two values of k_i used in this figure correspond to typical values for 1) normal acoustic dissipative losses and 2) MHD dissipation losses in the Stanford M-2 channel (see Fig. 1b).

In the actual case, changes in dissipation and phase velocity caused by MHD effects occur simultaneously. The dissipation effect can be measured more accurately because it is easier to detect the lowering of the peak level of the phase difference than it is to detect small shifts in the rising edge of the transitions.

Experimental Considerations

The change in the phase difference produced by MHD effects on both the dissipation and the phase velocity will be maximized if the measurements are made at as low a frequency as possible. For the phase velocity, it is obvious from Fig. 1 that the largest effects on $\bar{c}$ could be observed at low frequencies. For the dissipation the desirability of low frequencies is not as obvious because the value of k_i from this figure is relatively independent of frequency over the range of frequencies of interest. However the measurement of the magnetoacoustic effect on k_i really involves measuring the incremental magnetoacoustic dissipation in excess of the normal acoustic dissipation, as shown in Fig. 7. The classical expression for the amount of normal acoustic dissipation in a tube is[13]

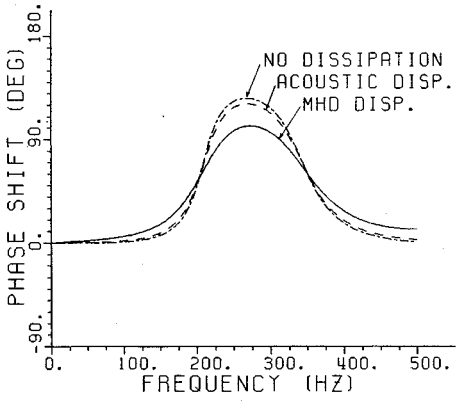

Fig. 7 Effect on the phase difference due to dissipation: 1) no dissipation, 2) normal acoustic dissipation, and 3) MHD dissipation (with $R_1=0.71$ for all three cases).

$$k_i=\frac{1}{2a_0}\left(\frac{\omega\nu}{2}\right)^{1/2}\frac{P}{S}\left(1+\frac{\gamma-1}{\sqrt{Pr}}\right) \tag{6}$$

where ν is the kinematic viscosity, P the perimeter of the duct, S the cross-sectional area of the duct, γ the ratio of specific heats, and Pr the Prandtl number of the gas. The acoustic dissipation scales with the square root of frequency, and hence the relative effect of the magnetoacoustic dissipation with respect to the normal acoustic value will be larger for lower frequencies.

Three methods were devised to produce transitions in the phase difference at the lowest possible frequencies. One method involved extending the test section beyond the active MHD channel. Because this arrangement tends to diminish the magnitude of the magnetoacoustic effects in the combined MHD duct and its continuation, the length of the extension must be limited. A second method involved the use of an enlarged cross-sectional area for the test section extension.

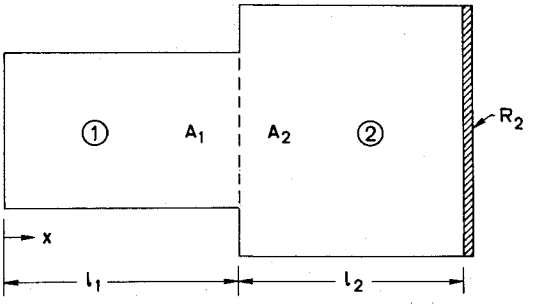

Fig. 8 Schematic of the two-region acoustic model.

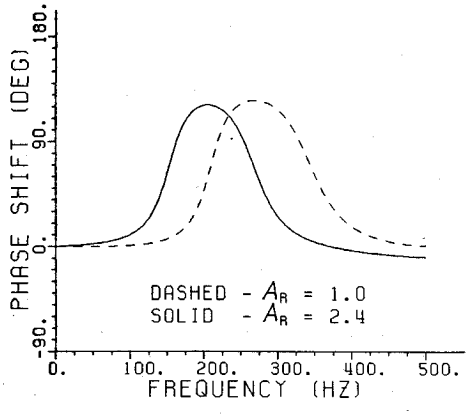

Fig. 9 Effect on the phase difference due to an area change (from 1.0 to 2.4) with $R_1 = 0.71$.

The effect of this area change on lowering the transition frequencies will be discussed in the next subsection. The third approach involved placing a small-area orifice at the downstream end of the test section extension just upstream of the exhaust ducting and adjusting the flow rate and back pressure so as to achieve choked flow in the orifice. For choked flow through an orifice, the acoustic reflection coefficient is[14]

$$R_{\text{orifice}} = (1-\alpha M)/(1+\alpha M) \tag{7}$$

where

$$\alpha = \frac{[1+(\gamma-1)M^2/2]}{[1+(\gamma-1)/2]}$$

The use of the choked-flow orifice as the downstream boundary of the test section has three advantages. First, it provides a known, constant downstream boundary condition. Secondly, it decouples the downstream exhaust acoustics (which had plagued preliminary magnetoacoustic experiments[16]) from the MHD channel acoustics. The third and most important property of the orifice is that the reflection coefficient of the downstream boundary is real and positive and hence approximates an acoustically closed end. The first transition frequency for a closed-end system is one-half that of an open-end system. An open-end system is approximately what would be obtained if the channel were to terminate through a diffuser (or otherwise) into the larger area exhaust ducting. This factor of two can make a significant difference particularly on the measurement of the magnetoacoustic effect on the phase velocity.

Two-Region Model

Equations (1-4) describe the acoustic properties of a highly simplied model of a MHD channel in which the duct area is constant and the gas properties are uniform in the axial direction. As described in the preceding subsection, the actual experimental arrangement is better modeled as consisting of two regions: an upstream region in which the waves are magnetoacoustic and a downstream region in which the waves are (ordinary) acoustic. A schematic of the two-region model is shown in Fig. 8. An area change at the interface between the regions has been included to lower the transition frequencies at which the phase difference changes. (The reason why the area change lowers the frequency of the transitions will be discussed later.)

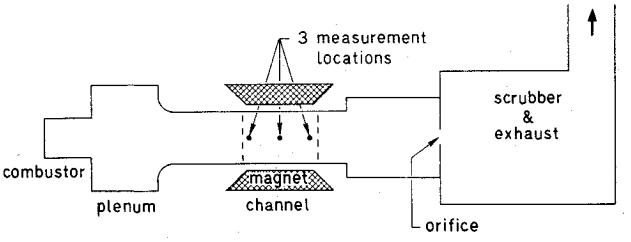

Fig. 10 Schematic of M-2 flowtrain used for the magnetoacoustic experiments.

The dependence of the phase difference on frequency for this two-region problem is obtained by employing the known solutions in each region separately and then applying the matching condition at the interface so that the pressure and volume flow rate are continuous. In ordinary acoustics, the specific acoustic impedance (ratio p'/u') is $\rho_0 a_0$, but in magnetoacoustics this is no longer true. The dispersion relationship must be used to determine the specific acoustic impedance, which may be different for the upstream- and downstream-traveling magnetoacoustic waves. To allow for this variable impedance, the equations are left generalized in terms of a normalized specific impedance, $z = p'/\rho_0 a_0 u'$.

The pressure and velocity fields in regions 1 and 2 can be expressed separately in an analogous form to Eq. (1). The coefficients for the velocity field are related to the coefficients of the pressure field by the known specific impedances for the upstream- and downstream-traveling waves. There are, therefore, four unknowns, two coefficients for each of the regions 1 and 2. The four conditions for determining these unknowns consist of upstream and downstream boundary conditions, and the two matching conditions at $x = \ell_1$,

$$p_1' = p_2', \quad u_1' A_1 = u_2' A_2 \tag{8}$$

The downstream boundary condition, expressed in terms of a complex reflection coefficient R_2, and the two matching conditions may be employed to obtain an expression for the reflection coefficient at $x = \ell_1$ in terms of the downstream reflection coefficient, the various specific impendances, and the area ratio, viz.,

$$R_1 = \frac{[1+\tilde{R}_2] - z_{12}A_R[1-z_{2R}\tilde{R}_2]}{z_{1R}[1+\tilde{R}_2] + z_{12}A_R[1-z_{2R}\tilde{R}_2]} \tag{9}$$

Here $\tilde{R}_2 = R_2 \exp\{i(k_{2u}+k_{2d})\cdot\ell_2\}$, and

$$z_{12} = \frac{z_{1d}}{z_{2d}}, \quad z_{1R} = -\frac{z_{1d}}{z_{1u}}, \quad z_{2R} = -\frac{z_{2d}}{z_{2u}}, \quad A_R = \frac{A_2}{A_1}$$

where the number subscript refers to region 1 or 2 and the letter subscript refers to the upstream- or downstream-traveling wave. More details on the derivation of Eq. (9) can be found in Ref. 15.

The impedance ratios represent impedance matching conditions at the interface. If the impedance ratios are one, the transfer efficiency at the interface is one, and there are no

reflections generated at the interface. If the impedance ratios are other than one, some reflection will occur at the interface, and it will effectively appear as if the downstream reflection coefficient R_2 has changed. Values for these impedance ratios can be obtained from the solution of the MHD dispersion relationship.

The solution for the pressure field in region 1 is then given by Eqs. (3) and (4) if the value for the reflection coefficient given in Eq. (9) is used in place of Eq. (2). When using Eqs. (3) and (4) for this two-region model, the lengths and wavenumbers that appear in these equations should be those for region 1 alone. All previous discussions about the nature and character of the phase difference plots still apply to the solutions obtained with this two-region model.

The increase in the cross-sectional area was included in the two-region model because of the effect it can have on reducing the first transition frequency at which the phase difference changes. As an example, Fig. 9 demonstrates the relative shift in the transition frequency caused by changing the area ratio A_R from 1.0 to 2.4. The 35% decrease in the first transition frequency produces a significant increase in the magnitude of the magnetoacoustic effects on both the damping coefficient and the phase velocities.

The decrease in the transition frequency occurs because the matching condition, Eq. (8), requires a discontinuity in u' and hence the specific acoustic impedance at the interface. The standing-wave envelope will also have a discontinuity at the interface which results in the first node moving closer to the downstream boundary. The change in the standing-wave envelope effectively reduces the wavelength at any given frequency, which causes the transition frequencies to shift to lower values.

The analysis for the effect of a sudden area change assumes purely one-dimensional flow. This description is obviously approximate, particularly in the vicinity of the area change. The model can be approximately corrected for two- and three-dimensional effects by using an effective value of A_R in the theory which is somewhat less than the geometrical value. The effective value of A_R can be found by performing a "calibration" measurement of the test section under known conditions. For these experiments, the calibration was done using room temperature nitrogen. Details on this calibration can be found in Ref. 15.

Experimental Apparatus and Procedures

Experimental Facility

All experiments were conducted in the Stanford M-2 MHD facility of the High Temperature Gasdynamics Laboratory. The flowtrain consisted of a combustor, plenum, nozzle, and run-in section upstream of the active MHD channel region. Downstream of the test section the run-out section had a cross-sectional area 2.7 times that of the active MHD region. The run-out was terminated by a choked-flow orifice followed by the scrubbing and exhaust system.

A schematic of the Stanford M-2 flowtrain used for these series of magnetoacoustic experiments is shown in Fig. 10. Some of the important flowtrain dimensions are listed in Table 1.

Table 1 Stanford M-2 flowtrain dimensions (in cm)

Combustor	Diam: 9.0; length: 37
Plenum	Width: 9.7; height: 22; length: 38
Nozzle	Inlet width: 6.0; inlet height: 13; exit width: 3.0; exit height: 10; length: 5
Channel	Width: 3.0; height: 10; length: 108
Run-out	Width: 6.6; height: 13; length: 51
Orifice	Width: 1.4; height: 6.8
Magnet	Active length: 50

Spacing between microphones in MHD channel: 21.9 cm
Distance from downstream microphone #3 to MHD channel exit: 17.1 cm

More details on the facility and characteristic parameters of the Stanford M-2 MHD generator can be found in Refs. 7 and 12. Details on the data acquisition instrumentation and equipment can be found in Ref. 16.

Excitation Source and Procedure

In the experimental MHD generator the pressure fluctuation level for the background noise portion of the inherent fluctuations can be comparable to the wave-like portion, especially at low-flow rates. This behavior occurs particularly at or near the transition frequencies in the phase difference, because these frequencies correspond to nodes in the acoustic part of the signals. (At a node the acoustic signal is greatly reduced, but the noise is unaffected.) The quality of the experimentally measured phase difference is greatly reduced when the background noise becomes comparable to or greater than the wave-like fluctuations. To produce good quality results, an excitation source is needed which is capable of producing acoustic-like disturbances in the MHD channel that are well above the background noise. Because the frequency spectrum of the noise is quite broad, the most effective approach is to use an excitation source that has a narrow-band frequency spectrum; then use spectral data reduction techniques to isolate the strong acoustic-like signal from the background noise. The simplest narrow-band excitation signal is one composed of a set of discrete frequencies. In reducing the data, only the results at the discrete excitation frequencies should be

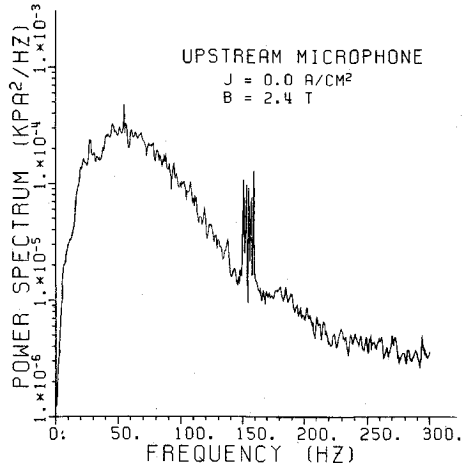

Fig. 11 Power spectral density of upstream microphone with the excitation source of five frequencies centered at 155 Hz.

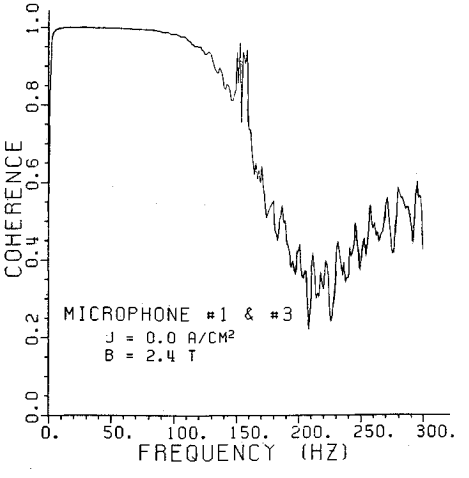

Fig. 12 Coherence between microphones with the excitation source of five frequencies centered at 155 Hz.

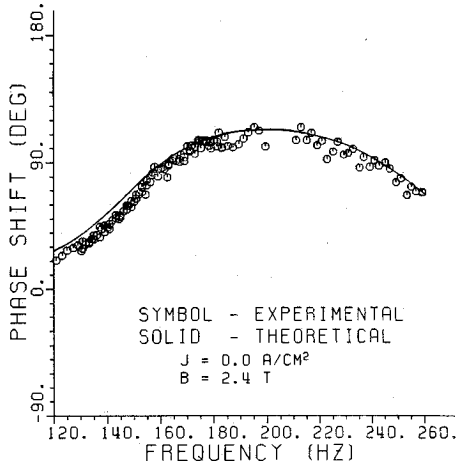

Fig. 13 Theoretical and experimental phase difference between microphones in the MHD channel for the ordinary acoustics case.

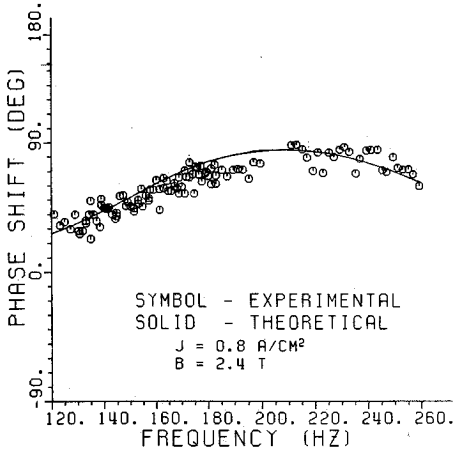

Fig. 14 Theoretical and experimental phase difference between microphones in the MHD channel for the magnetoacoustics case.

used, because the results at other frequencies are in general noisy and of poor quality.

To produce controlled acoustic-like disturbances in the MHD channel, a voltage was applied between opposed Faraday electrodes causing a large ac current, J', in the channel. The corresponding $J' \times B$ force on the plasma produced significant pressure fluctuations. The source of the oscillating current was a programmable dc power supply capable of producing up to 200 V and 20 A with an upper frequency bound of 3 kHz. The programming source for the power supply was a specially built sinewave synthesizer capable of producing a signal composed of up to 17 distinct sinewaves.

The number of sinewaves in the signal, the frequency spacing between each sinewave, and the center frequency of the signal were all adjustable. The values of these three parameters were selected on the basis of several physical considerations. For a fixed total power in the excitation source, the number of discrete frequencies in the signal controls the amount of power at each frequency. The more frequencies there are, the less power there is at each frequency. The maximum number of frequencies was set so that the induced acoustic-like signal in the plasma was still well above the background noise. The separation between the discrete frequencies controls the frequency resolution of the measurements. The bandwidth of the signal is equal to the number of discrete frequencies times the frequency separation. A larger bandwidth means fewer separate center frequencies are needed to cover the entire frequency range of interest. A tradeoff exists between higher resolution and larger bandwidth. To reduce the effects of possible drifts in the experimental conditions, it is desirable to keep the number of center frequencies small, and thereby keep the duration of the time requried to acquire the data small. Most of the data were acquired with either a 1 or 2 Hz frequency resolution and with five discrete frequencies used for each center frequency.

Experimental Results and Discussion

Results

Proper performance of the excitation source was critical to the success of the magnetoacoustic experiments. A typical power spectral density plot for the signal measured by the upstream pressure probe is shown in Fig. 11. The excitation frequencies for this case were centered around 155 Hz. These results show that the pressure signal produced by the source contains the desired narrow peaks at the discrete excitation frequencies and that the signals for the excitation frequencies are significantly above the background noise.

The introduction of a pressure oscillation in the plasma at a given frequency does not guarantee that the disturbance will be wave-like. The coherence (a measure of the portion of energy in one signal that is correlated to the energy in the other signal[17]) measured by two pressure probes at different locations in the channel can be employed to determine the extent to which the excited disturbance is propagational in character. A wave-like fluctuation produces a coherence of 1.0, while a noise fluctuation produces a low coherence of 0.2 or less. A typical coherence plot is shown in Fig. 12 for the same conditions as Fig. 11. The coherence is near one at low frequencies and drops off near the frequency at which the first node is located at the upstream pressure probe. The background coherence rises again after the frequency at which the first node passes the downstream pressure probe. The narrow peaks in the coherence around 155 Hz demonstrate that the excitation source is producing a strong wave-like disturbance that is spectrally well above the background noise.

The excitation frequencies were incremented to cover the range of frequencies from 120 to 260 Hz, which spans the range of the first transition as shown in Fig. 9. The phase difference at each excitation frequency between the upstream and the downstream pressure probes determined for the cases of ordinary acoustics and of magnetoacoustics is shown in Figs. 13 and 14, respectively. Included in these figures is the corresponding theoretical value computed using the two-region model and the MHD dispersion relationship. The experimental MHD conditions are identical to those depicted in Fig. 1. For both figures the presence of the magnetic field was necessary for proper operation of the excitation source. The presence of both a magnetic field and some current flowing in the plasma are necessary for a magnetoacoustic interaction to occur of the type predicted by the theory presented in this paper.

Discussion

As may be seen in Figs. 13 and 14, the experimental data and the theory are in good agreement. The phase difference dependence on frequency without and with current, shown separately in Figs. 13 and 14, changes significantly. The peak value of the phase difference is reduced from 110 deg in the normal acoustic case to 85 deg in the magnetoacoustic case. The differences between the two figures are mostly due to an increase in k_i of about 0.13 for the magnetoacoustic waves, compared to a value of about 0.03 for the normal acoustic waves. The predicted changes in the phase velocities are relatively small (less than 5% in the measured range of frequencies) and could not be determined from the present data owing to the scatter shown in Fig. 14. The relatively large Faraday load factor was responsible for the small effect on the phase velocities. The external load resistor used in the experiments was only 0.7 Ω, but the large boundary layer

resistances were responsible for the high value of the effective Faraday load factor.

Future work will concentrate on refining the data-reduction procedures employed for the present measurements and on analyzing additional data to examine the consistency of the model. An analysis of additional data acquired during these experiments will be used to test the consistency of the model by comparing the phase difference between different pairs of pressure probes measured at the same time and by comparing phase differences between the same pressure probes measured under different MHD conditions. The latter analysis will be particularly important in determining the effect of the magnetic interaction parameter on the damping factor k_i.

Conclusions

Interactions between the magnetoacoustic fields and the electrical power circuitry can have detrimental effects on the performance of large-scale MHD generators. Previous theoretical studies of these interactions have been based primarily on examining the solutions of an MHD dispersion relationship. The derivation of this relationship contains many assumptions and approximations whose validity has never been successfully tested experimentally. The magnitude of the magnetoacoustic effects in laboratory-scale MHD generators is small, but experiments to compare with the theory can be performed by making measurements at low frequencies where the predicted effects are the largest.

A simple acoustic model of the experimental MHD generator has been developed and used in conjunction with the MHD dispersion relations to predict the pressure field in the MHD generator. An experimental approach using the phase difference between pressure signals measured at different locations in the MHD channel to detect small MHD effects on both the damping and the phase velocity of magnetoacoustic waves has been developed and has proven to be quite sensitive to small changes. To make these measurements, propagating low-frequency pressure fluctuations in an MHD channel were excited using a specially designed external power source to produce oscillations in the current between a pair of opposed electrodes located upstream of the MHD channel. Analysis of the data shows good agreement between the measured and predicted MHD effect of wave amplitude damping on the phase difference. The predicted changes in the phase velocities of the waves were too small to detect owing to the scatter in the data. The measurements reported here are believed to be the first to provide experimental support for the predicted MHD effects on acoustic waves.

Acknowledgments

This work was supported by the National Science Foundation under Grant NSF-CPE-82-17622 and by the U.S. Department of Energy under Contract DE-AC22-84PC-70509.

References

[1]Velikov, E.P., "Hall Instability of Current-Carrying Slightly-Ionized Plasmas," *Proceedings of the Symposium on MHD Electrical Power Generation,* The Symposium on Engineering Aspects of MHD, Inc., Newcastle-upon-Tyne, England, 1962, pp. 135–136.

[2]Wright, J.K., "A Temperature Instability in MHD Flow," *Proceedings of the Physics Society,* Vol. 81, 1963, pp. 498–505.

[3]McCune, J.E., "Wave Growth and Instabilities in Partially-Ionized Gases," Paper 33, *Proceedings of the International Symposium on MHD Electrical Power Generation,* The Symposium on Engineering Aspects of MHD, Inc., Paris, 1964.

[4]Locke, E.V. and McCune, J.E., "Growth Rates for Axial Magneto-Acoustic Waves in a Hall Generator," *AIAA Journal,* Vol. 4, Oct. 1966, pp. 1748–1751.

[5]Powers, W.L. and Dicks, J.B., "Transient Wave Growth in MHD Generators," *AIAA Journal,* Vol. 6, June 1968, pp. 1007–1012.

[6]Fishman, F.J., "Instabilities of Hall MHD Generators to Magneto-Acoustic Waves," Avco Everett Research Lab Rept. 323, Everett, MA, Feb. 1969.

[7]Barton, J.P., "Fluctuations in Combustion-Driven MHD Generators," High Temperature Gasdynamics Laboratory Rept. 118, Stanford University, Stanford, CA, Aug. 1980.

[8]Barton, J.P., Koester, J.K., and Mitchner, M., "An Experimental Investigation of Fluctuating Properties Within a Combustion MHD Generator," *16th Symposium on Engineering Aspects of Magnetohydrodynamics,* Pittsburgh, PA, May 1977, pp. VII. 5.27–VII. 5.33.

[9]Barton, J.P., Koester, J.K., and Mitchener, M., "An Experimental and Analytical Investigation of Fluctuation Phenomena Within a Subsonic Combustion MHD Generator," *17th Symposium on Engineering Aspects of Magnetohydrodynamics,* Stanford Univ., Stanford, CA, March 1978, pp. E.5.1–E.5.8.

[10]Barton, J.P., Koester, J.K., and Mitchner, M., "Fluctuations in Combustion MHD Generator Systems," *18th Symposium on Engineering Aspects of Magnetohydrodynamics,* Butte, MT, June 1979, pp. J.1.1–J.1.8.

[11]Koester, J.K., Farrar, L.C., Wood, P., and Ferraro, R.J., "Integrated MHD Generator-Inverter System Test Results at CDIF," *Proceedings of the 21st Symposium on Engineering Aspects of MHD,* Argonne, IL, 1983, pp. 2.3.1–2.3.14.

[12]Simons, T.D., "Acoustic and Entropy Waves in a Combustion MHD Generator," High Temperature Gasdynamics Laboratory Rept. 203, Stanford University, Stanford, CA, June 1982.

[13]Temkin, S., *Elements of Acoustics,* 1st ed., Wiley, New York, 1981, p. 417.

[14]Davis, S., "Transmission of Sound from a Nozzle Carrying a Compressible Subsonic Flow," Paper presented at the 86th meeting of the Acoustical Society of America, Los Angeles, Oct.–Nov. 1973.

[15]Munce, A.C. Jr., Mitchner, M., and Koester, J.K., "Magneto-acoustic Phenomena in MHD Generators," *Proceedings of the 22nd Symposium on Engineering Aspects of MHD,* Mississippi State Univ., State College, MS, 1984, pp. 2:2:1–2:2:19.

[16]Munce, A.C. Jr., Mitchner, M., and Koester, J.K., "Magneto-acoustic Effects on Phase Velocities of Waves in MHD Generators," *Proceedings of the 21st Symposium on Engineering Aspects of MHD,* Argonne, IL, 1983, pp. 3.3.1–3.3.13.

[17]Bendat, J.S. and Piersol, A.G., *Random Data: Analysis and Measurement Procedures,* 1st ed., Wiley-Interscience, New York, 1971, p. 142.